https://doi.org/10.1007/s41230-026-5016-6

Titanium alloy with synergistic enhancement of strength and toughness based on molybdenum equivalent design: Microstructure evolution and strengthening-toughening mechanism

Yi-li Li[1], **Hong-ze Fang[1], *Rui-run Chen[1], Jia-qi Hao[1], Bao-hui Zhu[2], and Jing-jie Guo[1]

1. National Key Laboratory for Precision Hot Processing of Metals, Harbin Institute of Technology, Harbin 150001, China

2. Ningxia Horizontal Titanium Industry Co., Ltd., Shizuishan City, Ningxia 753000, China

Abstract: The traditional "trial and error" microstructural control method, with high cost and low efficiency, has become a key issue restricting the development of ultra-high strength and toughness titanium alloys. This study adopts the molybdenum equivalent ($Mo_{[eq]}$) method to rapidly design Ti-*x*Mo-4Al-4Zr-3Nb-2Cr-1Fe alloys (*x*=5–9). The as-cast alloys with different $Mo_{[eq]}$ exhibit a single peak of the β phase in XRD. The β grains of 5Mo alloy (the lowest $Mo_{[eq]}$) exhibit elongated columnar grain characteristics. As the $Mo_{[eq]}$ increases, the β grains transition towards a more equiaxed form, resulting in a decrease in aspect ratio and a reduction in grain size. As the $Mo_{[eq]}$ increases, the α phase content gradually decreases and the α phase is almost unobservable in 9Mo alloy (the highest $Mo_{[eq]}$). The α phase in 5Mo alloy exhibits short rod-shaped shapes with an average length of about 2.4 μm, while the α phase in 6Mo alloy shows an equiaxed and short rod shapes with the smallest size. The strength, plasticity, and toughness are the lowest in 5Mo alloy, with values of 867 MPa, 7.3%, and 56 MPa·$m^{1/2}$, respectively. However, it reaches its maximum in 6Mo alloy, where the strength, plasticity, and toughness increase to 984 MPa, 12.8%, and 74 MPa·$m^{1/2}$, respectively. The mechanical properties of Ti-*x*Mo-4Al-4Zr-3Nb-2Cr-1Fe alloys are affected mainly by solid-solution strengthening of Mo element, refinement of β grain, and changes in α/β phase content. This study lays a certain theoretical foundation for the theoretical research and composition development of new ultra-high strength and toughness titanium alloys.

Keywords: titanium alloy; ultra-high strength and toughness; $Mo_{[eq]}$; microstructure evolution; strengthening and toughening mechanism

CLC numbers: TG146.23 **Document code:** A **Article ID:** 1672-6421(2026)02-245-09

1 Introduction

With the rapid development of the aerospace industry, the requirements for structural materials for aerospace are increasingly focused on lightweight, high strength, and high toughness[1-4]. To adapt to this development trend, ultra-high strength and toughness titanium alloys (tensile strength>1,300 MPa, fracture toughness> 55 MPa·$m^{1/2}$), as high-performance lightweight metals, are becoming a highly valued new structural material in the field of high-tech new materials[5-8]. It is widely recognized that ultra-high strength and toughness titanium alloys, as a typical structural material, are characterized by three fundamental properties: strength, plasticity, and fracture toughness. Achieving an optimal balance among these properties is inherently challenging[9-11], as their interdependence presents a well-documented contradiction in metallurgy. Due to inherent contradictions at the source, ultra-high

*Rui-run Chen

Ph. D., Professor, Doctoral Supervisor. He is the winner of the National Science Fund for Distinguished Young Scholars, and one of the leading talents of the scientific and technological innovation of the "Ten-thousand Talents Program". His research interests primarily focus on the solidification theory and casting technology of titanium aluminum alloys, niobium silicon alloys, high entropy alloys, metal based hydrogen storage materials, and solar grade silicon. To date, he has published more than 240 SCI indexed papers, and has been authorized 24 patents for inventions of China.

E-mail: ruirunchen@hit.edu.cn

**Hong-ze Fang

E-mail: fanghongze@hit.edu.cn

Received: 2025-01-18; Revised: 2025-04-18; Accepted: 2025-11-28

strength and toughness titanium alloys are currently almost completely in a bottleneck period of development and have not been able to be truly applied. However, research on higher strength titanium alloys exceeding 1,300 MPa has never been interrupted[12-15]. Researchers continuously strive to improve material properties on the basis of matching strength and toughness through microstructural design and optimized element configurations.

Typically, ultra-high strength and high toughness titanium alloys exhibit an α+β two-phase microstructure, wherein the α precipitation phase serves to reinforce the β phase matrix[16-18]. The mechanical properties of alloys depend on the properties of the two phases and their matching. Achieving precise control over the composition, proportion, and morphology of these phases is essential for the comprehensive optimization of alloy strength and toughness[19-21]. The most fundamental aspect of alloy design is composition design[22-24]. Ultra-high strength and toughness titanium alloys often have 5–8 alloying elements. This is because different elements have different contributions to the mechanical/physical properties, process performance, and cost of alloys[25,26]. The traditional "trial and error" microstructural control method, with high cost and low efficiency, has become a key issue restricting the development of ultra-high strength and toughness titanium alloys. Therefore, the appropriate and rapidly selection of these elements remains a focal point of research in the field.

From the perspective of alloy composition design, the molybdenum equivalent ($Mo_{[eq]}$) serves as a critical parameter in the context of β-Ti alloys, as it influences the quantity and stability of the metastable β phase that can be preserved during quenching processes[27,28]. Typically, a $Mo_{[eq]}$ value of at least 10 is required to ensure the stabilization of the β phase during quenching[29,30]. From previous studies, when the $Mo_{[eq]}$ is maintained within the range of 9 to 15, the alloy exhibits elevated strength in both annealed and solution-aged conditions. Conversely, values of $Mo_{[eq]}$ that are either too high or too low do not facilitate strength enhancement[31]. This phenomenon can be attributed to the fact that within the 9 to 15 range, the ratio of α to β phases in titanium alloys approaches 1:1, resulting in mutual constraints between the two phases. This interaction inhibits grain growth, which is advantageous for enhancing the strength and toughness of the alloy, while simultaneously increasing the α/β interface area, which is an essential and effective mechanism for impeding dislocation movement in β-type titanium alloys.

Therefore, the $Mo_{[eq]}$ method was used to efficiently screen for the optimal composition range of titanium alloys with high strength and toughness potential in this study, which can be expanded to high strength and toughness designs in all titanium alloy fields. The Ti-*x*Mo-4Al-4Zr-3Nb-2Cr-1Fe (Ti*x*44321) alloy system is selected as the target for investigation based on the previous work by our team[32]. The effects of Mo element on the phase constitution, microstructure evolution, β grain size were explored, and corresponding strengthening and toughening mechanism of the titanium alloy were also revealed. The aim is to provide high-quality ingots for designing ultra-high strength and toughness β titanium alloys based on in-depth research on some basic issues of Mo element doping, and lay a certain theoretical foundation for the theoretical research and composition development of new ultra-high strength and toughness titanium alloys.

2 Materials and methodology

The designed alloys Ti-*x*Mo-4Al-4Zr-3Nb-2Cr-1Fe alloy (hereinafter referred to as 5Mo, 6Mo, 7Mo, 8Mo, and 9Mo) were prepared utilizing a vacuum non-consumable melting furnace with a water-cooled copper crucible. The melting procedure was executed five times to achieve a homogeneous composition. The phase types present in the alloys were analyzed employing an X-ray diffractometer, specifically the Empyrean model. The microstructural characteristics of all alloys were examined using a Quanta 200F field emission scanning electron microscope, manufactured by FEI. Statistical analysis of the microstructure features was performed using Image Pro Plus 6.0 software. Additionally, fine microstructure morphology was observed with a Talos F200X transmission electron microscope.

The tensile properties and fracture toughness of the alloy were evaluated using an Instron 5569 electronic universal testing machine. The tensile specimens were designed in a dog bone shape measuring 30 mm×2.2 mm×2 mm. The room temperature fracture toughness test was conducted in accordance with ASTM E-399 standard, using a single-sided cut three-point bending specimen with dimensions of 20 mm (L)× 4 mm (W)×2 mm (B), and a U-shaped notch with a depth of 2 mm was prefabricated at the center of the sample. The loading rates set at 1 $mm \cdot min^{-1}$ for the tensile tests and 0.5 $mm \cdot min^{-1}$ for the toughness assessments. Each sample was conducted three times to ensure the reliability of the results, and the average value was taken as the final result.

$Mo_{[eq]}$ is an important approach for the composition design of titanium alloys, and its calculation equation is as follows:

$$Mo_{[eq]}=\%Mo+\%Ta/4+\%Nb/3.3+\%W/2+\%V/1.4+\%Cr/0.6+\%Ni/0.8+\%Mn/0.6+\%Fe/0.5+\%Co/0.9\ (wt.\%) \quad (1)$$

In this study, only the content of Mo was the variable, the $Mo_{[eq]}$ value of the alloy system is solely related to the Mo content. According to the above formula, the $Mo_{[eq]}$ is calculated, and the results are shown in Table 1. The $Mo_{[eq]}$ value of this alloy system is between 11 and 16, and it increases linearly with the increase of Mo content. The $Mo_{[eq]}$ of 5Mo–8Mo alloy is within the theoretically optimal range (9–15), while 9Mo alloy, as a comparison, exceeds the optimal range.

Table 1: $Mo_{[eq]}$ value of as-cast Tix44321 alloy with different Mo contents

Alloy	5Mo	6Mo	7Mo	8Mo	9Mo
$Mo_{[eq]}$	11.24	12.24	13.24	14.24	15.24

3 Results

3.1 Content and size of α/β phase and dislocations at α/β phase interface

As one of the most important β-stabilizing elements, the content of α and β phases is closely related to Mo content. Therefore, XRD technology was used to investigate the phase constitution of alloys with different Mo contents, and the results are shown in Fig. 1. The alloys with different Mo contents exhibit a single peak of the β phase, and no characteristic peak of the α phase is observed. This phenomenon indicates that the high β stability coefficient of the alloy system results in a diminished α phase content and the characteristic peak of the β phase is much higher compared to the α phase. In addition, no characteristic peaks of other phases are observed, confirming that all Mo elements dissolve into the interior of the two phases and no new phases form, indicating that Mo primarily contributes to solid solution strengthening during subsequent strengthening processes. Although no significant presence of α phase is observed in the as-cast state by XRD, the Mo equivalent of these alloys is in the range of 11–16, which helps to form a 1:1 ratio of α/β after hot working.

The XRD diffraction peaks of alloys with different Mo contents exhibit two different points. Firstly, there is a rightward shift in the β phase peak as Mo content increases. In addition, the β phase consistently exhibits a (110) preferred orientation across all Mo contents. Specifically, both the 5Mo and 7Mo alloys show only the (110) diffraction peak. In contrast, the 6Mo alloy not only retains the (110) peak but also displays a notably intense (211) peak. As the Mo content further increases, the intensity of the (211) peak decreases. Moreover, when the Mo content exceeds 8wt.%, a (200) peak emerges. These observations indicate that variations in Mo content not only influence the β phase content but also modify the orientation of the β phase. Considering that the atomic radius of Mo atoms is 0.136 nm, which differs by 6.2% from the atomic radius of titanium (Ti) atoms at 0.147 nm, the incorporation of Mo is likely to induce lattice distortion within the alloy. The partial enlarged image near the peak of (110), as shown in Fig. 1(b), confirms the obvious rightward shift of this peak and the lattice distortion caused by the solid solution of Mo element.

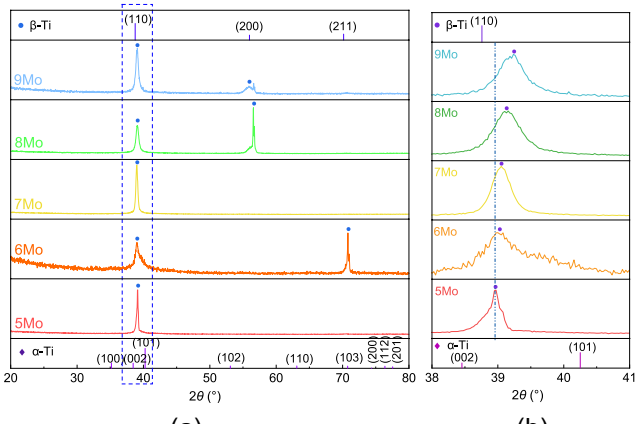

Fig. 1: XRD patterns (a) and partial enlarged image (b) of as-cast Tix44321 alloy with different Mo contents

In addition to the phase constitution, the Mo content inevitably affects the β grain size, α phase morphology, and the ratio of α and β phases in titanium alloys. Therefore, SEM was used to observe the alloy microstructure under different Mo contents, and the results are shown in Fig. 2. The morphology and size of β grains in as-cast titanium alloys are one of the key factors affecting their mechanical properties, so the β grains are firstly observed at low magnification. Alloys with different Mo contents all have coarse β grains, which is one of the main limiting factors for further improving the strength of as-cast titanium alloys. The β grains of 5Mo alloy exhibit elongated columnar grain characteristics, with the largest grain size at about 650 μm. As the Mo content increases to 6Mo alloy, the β grains transition into a more equiaxed form, resulting in a decrease in aspect ratio and a reduction in grain size, reaching a minimum of about 362 μm at 6Mo alloy. However, with further increases in Mo content, the equiaxed degree of β grain morphology decreases and the size increases.

Observing the α phase inside the β grain (as shown in the orange circle in Fig. 2) at high magnification and combining it with XRD data to statistically analyze the phase content of the two phases, it is evident that as the Mo content increases, the α phase content gradually decreases from 11% in the 5Mo alloy to almost unobservable in the 9Mo alloy. The 9Mo alloy presents a clean and pure β phase state. In addition, the distribution of α phase inside the β grains is not uniform and exhibits a random distribution characteristic. At higher magnifications, it is observed that in addition to the phase content, the morphology of the α phase also changes with the increase of Mo content. The α phase in 5Mo alloy exhibits short rod-shaped shapes with slightly larger aspect ratios, with an average length of about 2.4 μm. When the Mo content exceeds 6wt.%, the α phase gradually shows an equiaxed and short spherical, and the α phase size decreases accordingly. When the Mo content continues to increase to 7wt.%, the α phase achieves a fully spheroidized state, and the size is further refined. Subsequent increases in Mo content do not influence the size or morphology of the α phase, but rather result in a continued decrease in the content of the α phase.

The microstructure of 5Mo and 9Mo alloys was observed using TEM, and the results are shown in Fig. 3. For 5Mo alloy, the randomly observed α phases at different positions are distributed in a long strip shape with a great aspect ratio, and the distribution is uneven. Most of them are arranged in a parallel state without directionality, which is consistent with the phenomenon observed in SEM images. There are not many dislocations observed inside the alloy, mostly concentrated at the phase α/β interface, existing in the form of single dislocation lines or arranged as dislocation walls. In 9Mo alloy, a large area of pure β phase structure is observed, with a clean interior and almost no presence of α phase. In addition, due to the lack of second phase or precipitated phase, there are almost no defects such as dislocations in 9Mo alloy.

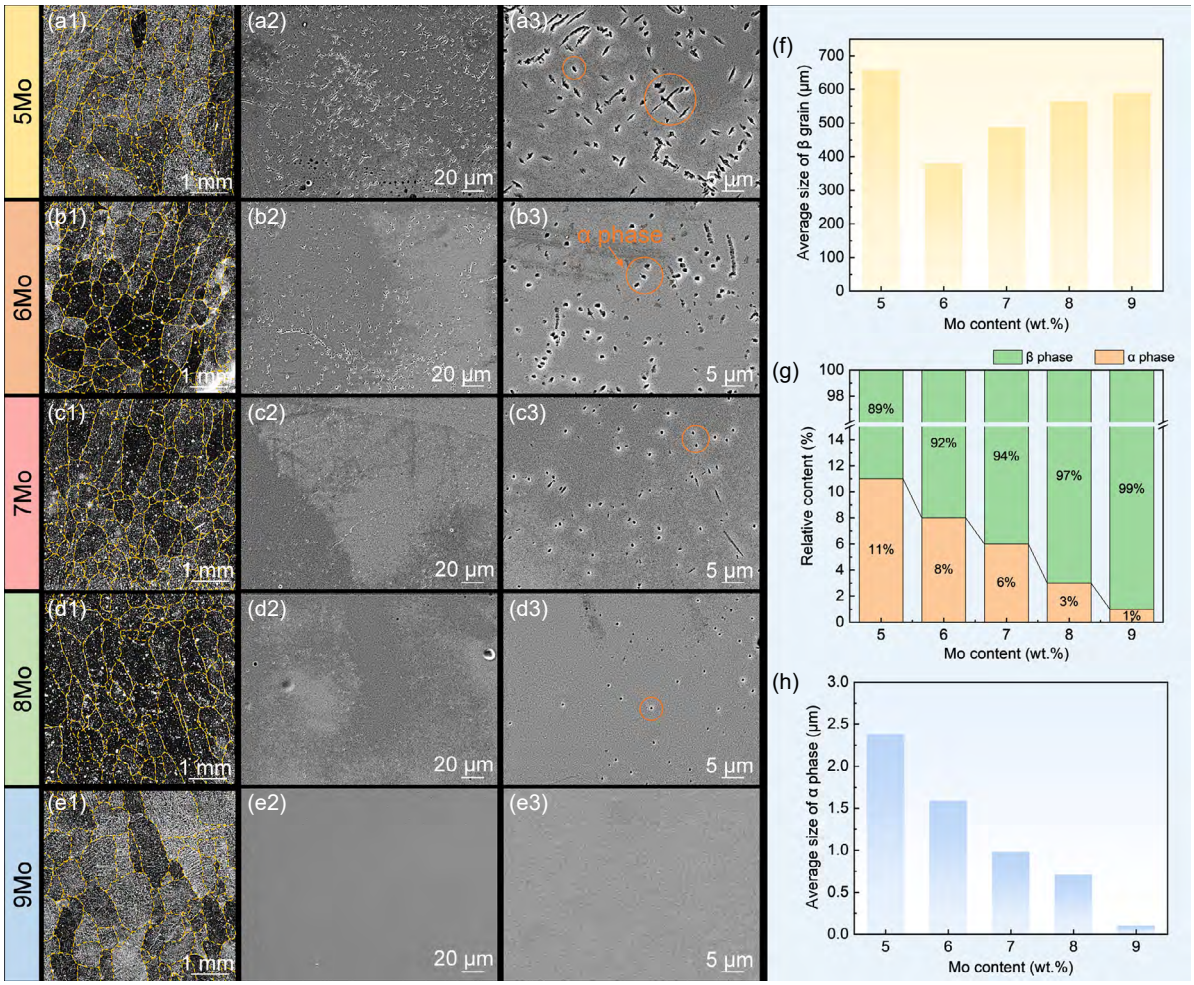

Fig. 2: SEM microstructure images and related data statistics of as-cast Ti*x*44321 alloys with different Mo contents: (a1–a3) 5Mo alloy; (b1–b3) 6Mo alloy; (c1–c3) 7Mo alloy; (d1–d3) 8Mo alloy; (e1–e3) 9Mo alloy; (f) average size of β grains; (g) relative content of α and β phases; (h) average size of α phase

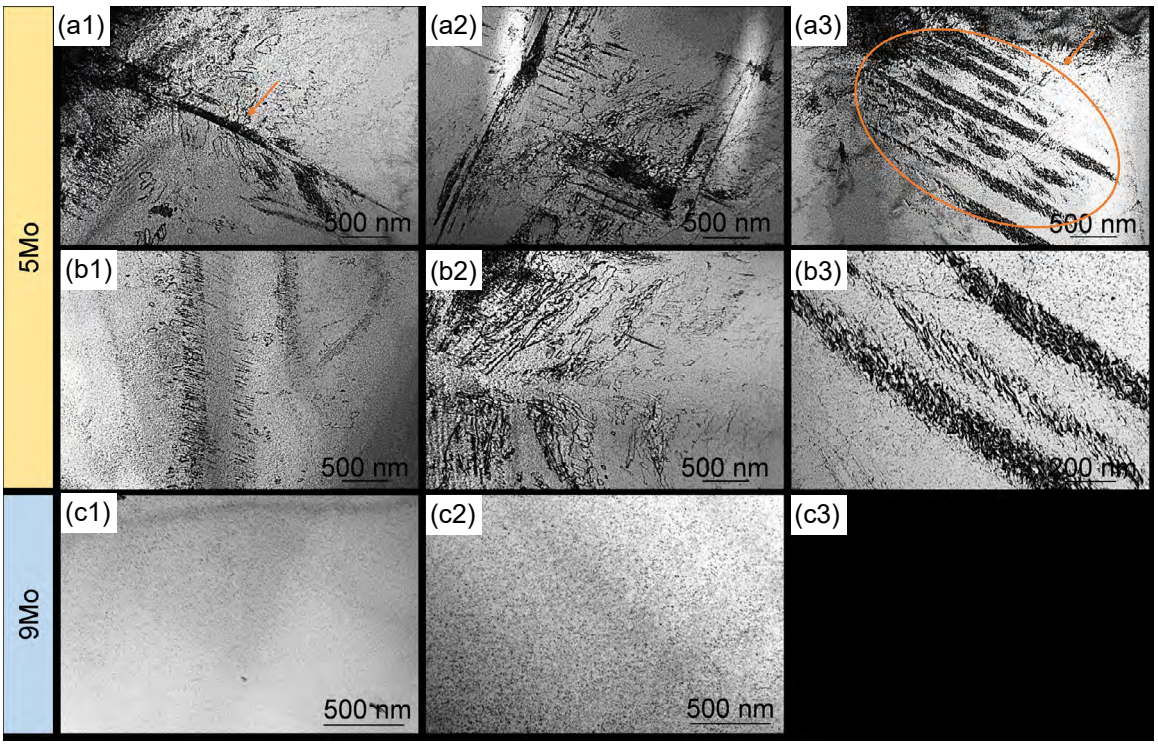

Fig. 3: TEM microstructure images of as-cast Ti*x*44321 alloys with different Mo contents: (a1–a3) morphology of α phase in 5Mo alloy; (b1–b3) dislocations in 5Mo alloy; (c1–c3) microstructure of 9Mo alloy

3.2 Tensile strength, strain, and fracture toughness

Due to the solid solution effect of Mo element on the microstructure, the mechanical properties of alloys with different Mo contents are inevitably different. The tensile properties were tested, and the results are shown in Fig. 4. Alloys with different Mo contents exhibit the tensile strength fluctuating in the range of 800–1,000 MPa. Compared to tensile strength, the change in tensile strain is greater, increasing from a minimum of 7% to a maximum of nearly 13%, almost doubling the plasticity. In addition, a rare phenomenon of synergistic improvement in strength and plasticity is observed in this alloy system. The strength and plasticity are the lowest in the 5Mo alloy, with values of 867 MPa and 7.3%, respectively. It reaches its maximum in the 6Mo alloy, where the strength and plasticity increase to 984 MPa and 12.8%, respectively. At this point, the strength increases by 13.5% and the plasticity increases by 75.3%. This phenomenon indicates that the increase in Mo element has a greater effect on the plasticity of the alloy Subsequently, as the Mo content continues to increase, both the strength and plasticity decrease.

The fracture toughness of the as-cast Ti*x*44321 alloy was tested, and the results are shown in Fig. 5. The fracture toughness reaches a minimum value of 56 MPa·m$^{1/2}$ in the 5Mo alloy, and reaches a maximum value of 74 MPa·m$^{1/2}$ when the Mo content increases to 6wt.%. At this point, the fracture toughness of the alloy increases by 32.1%, and then shows a decreasing trend with the continued increase of Mo content. The fracture toughness of all alloys exceeds 55 MPa·m$^{1/2}$, meeting the requirements of high toughness titanium alloys.

Based on the comprehensive design criteria of $Mo_{[eq]}$ and the variation law of strength and toughness, within the $Mo_{[eq]}$ range of 11–16, the strength and toughness show a trend of firstly increasing and then decreasing with the increase of $Mo_{[eq]}$. Specifically, when the $Mo_{[eq]}$ is in the range of 12–14, it is most advantageous to obtain alloys with high strength toughness matching, corresponding to a Mo content within the range of 6wt.%–8wt.%. And in this range, it can even meet the requirements of ultra-high toughness in the as-cast state, indicating that this alloy system has great potential as a candidate alloy system for ultra-high strength and toughness titanium alloys. In particular, 6Mo alloy is the most suitable candidate alloy component for ultra-high strength and toughness titanium alloys.

The tensile fracture surface and crack propagation path of alloys with different Mo contents are shown in Fig. 6. The macroscopic tensile fracture of 5Mo alloy shows obvious intergranular fracture characteristics, indicating that the fracture mode of the alloy is brittle fracture. After magnification, a stepped river pattern is observed in the microstructure, and a very small number of dimples are observed at the grain boundaries, as shown by the orange circle in Fig. 6(a2), which improve the plasticity of the alloy to a certain extent. As the Mo content increases, there is a corresponding improvement

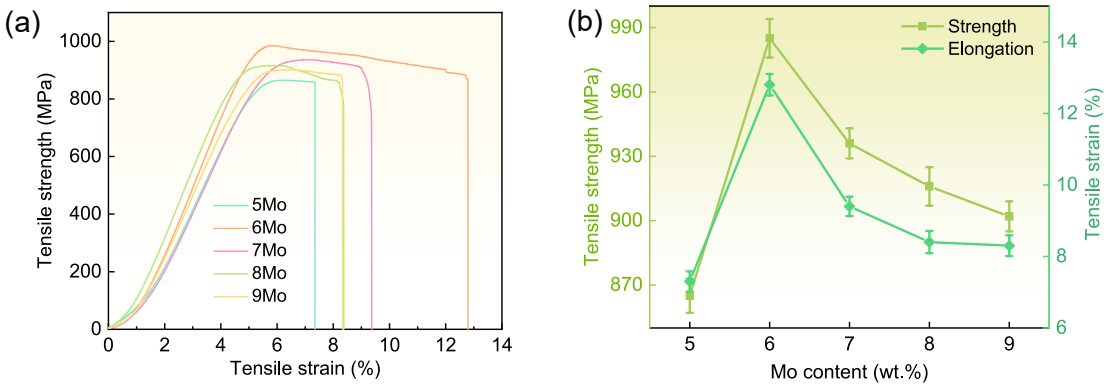

Fig. 4: Tensile curves and corresponding tensile strength and strain of as-cast Ti*x*44321 alloys with different Mo contents: (a) tensile curves; (b) tensile strength and strain

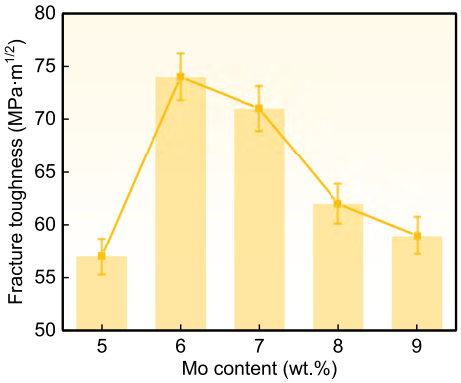

Fig. 5: Fracture toughness of as-cast Ti*x*44321 alloys with different Mo contents

in plasticity, characterized by a greater density of smaller dimples at the fracture surface, with the grain size associated with intergranular fracture being smaller than that observed in the 5Mo alloy. The 7Mo alloy, which demonstrates the second highest level of plasticity, similarly exhibits dense dimples and river patterns. However, with further increases in Mo content, a reduction in the number of dimples is noted, and the intergranular fracture mode becomes increasingly pronounced.

Analysis of the crack propagation path reveals that the 6Mo alloy, which exhibits the highest toughness, possesses the most complex crack trajectory and the longest crack length. Furthermore, pronounced extrinsic toughening features, such as crack bridging and branching, are observed in 6Mo alloy.

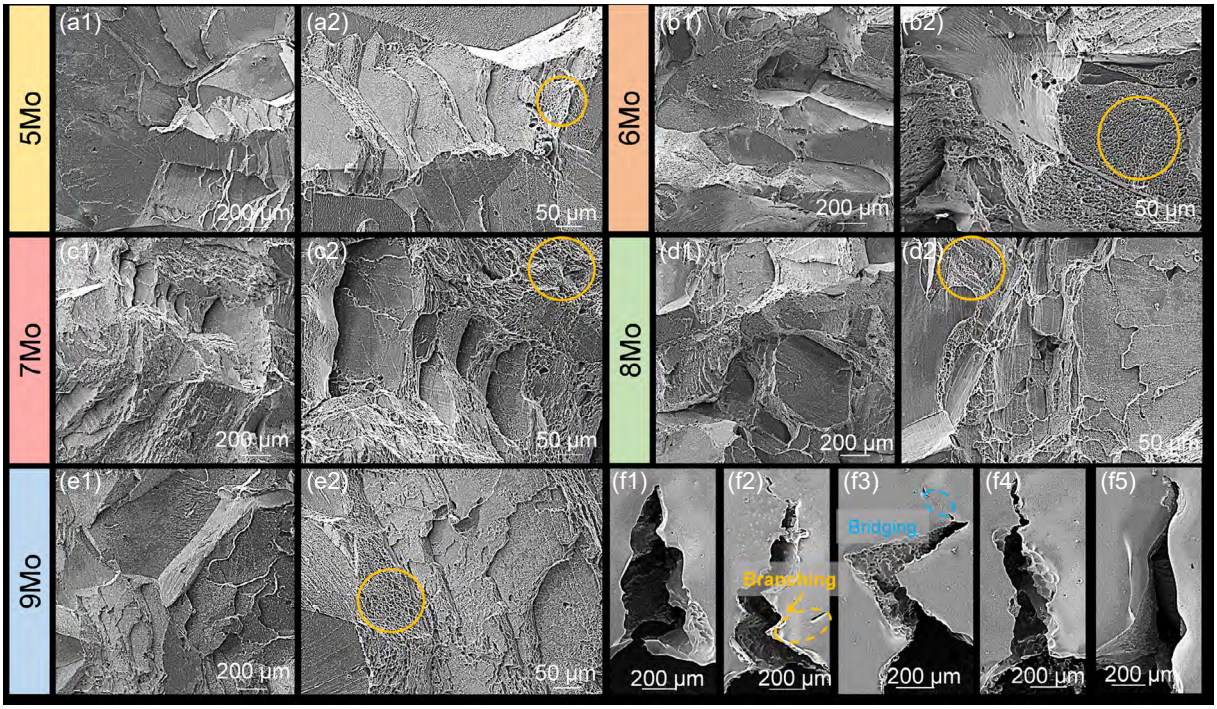

Fig. 6: Tensile fracture morphology (a1–e2) and fracture toughness crack propagation path (f1–f5) of as-cast Ti*x*44321 alloys with different Mo contents: (a1–a2) 5Mo alloy; (b1–b2) 6Mo alloy; (c1–c2) 7Mo alloy; (d1–d2) 8Mo alloy; (e1–e2) 9Mo alloy; (f1) 5Mo alloy; (f2) 6Mo alloy; (f3) 7Mo alloy; (f4) 8Mo alloy; (f5) 9Mo alloy

These extrinsic toughening mechanisms are also identified in 7Mo alloy, which ranked second in toughness. Conversely, the crack propagation paths of the 5Mo and 9Mo alloys, which exhibit lower toughness, are characterized by reduced tortuosity and shorter lengths, with no external toughening features identified, resulting in lower toughness.

4 Discussion

The results show that variations in Mo content within the as-cast Ti*x*44321 alloys predominantly influence the size and morphology of β grains, the proportion of α/β phases, and exert a minor effect on the α phase morphology. These changes lead to changes in the strength, toughness, and plasticity of the alloy. Specifically, the β grain size of the alloy firstly decreases and then increases with the increase of Mo content, reaching a minimum value at 6wt.%; while the strength, plasticity, and toughness of the alloy firstly increase and then decrease with increasing Mo content, reaching a maximum value at 6wt.%. The following analysis provides a concise overview of the factors influencing the microstructure and mechanical properties of the as-cast Ti*x*44321 alloys containing Mo.

4.1 Reasons for grain refinement and the decrease in α phase content

Firstly, the negative mixing enthalpy between Mo and other elements (such as Ti, Zr, and Nb)[33] in the alloy leads to the release of heat during the solidification process, partially offsetting the effect of structural undercooling and promoting the formation of equiaxed grains. Due to the existence of smaller β grain size in the 6Mo alloy, the grain growth rate under isothermal conditions can be expressed as[34]:

$$\frac{\mathrm{d}D}{\mathrm{d}t}=k_1 D^{-1} e^{-\frac{Q}{RT}} \tag{2}$$

where D is the grain size, t is time, k_1 is a constant, Q is the activation energy for grain growth, R is the gas constant, and T is the absolute temperature. Many studies have been conducted[35,36] to investigate the activation energy of grain growth in titanium alloys. The difference in activation energy for grain growth is mainly attributed to β phase transition temperature (T_β) or element addition. The decrease of T_β and the increase of Mo content will increase the activation energy of grain growth in this alloy system. Therefore, when the Mo content is appropriately increased, the β grains are refined to a certain extent. In addition, the increased Mo solute atoms also to some extent inhibit the migration of β grain boundaries and increase the resistance to grain growth[37].

Secondly, our results indicate that not only is the crystal structure of the alloy system sensitive to Mo content, but the morphology of the α phase is also influenced by Mo content. When the Mo content in the system increases to 9wt.%, the β phase becomes the only dominant phase. This change in phase content can be attributed to the difference in atomic radii (11 pm) between the solute atoms, Mo and Ti, which results in the dissolution of Mo within the Ti matrix and a consequent reduction in lattice parameters. Such changes may lead to variations in the morphology of the α phase during the β→α phase transition process[38]. It is well established that the α phase is formed from the β phase during the cooling process of the alloy, and the content of the α phase largely depends

on the stability of the β phase. As the Mo content increases, the stability of the β phase improves, and the transition temperature from β phase to α phase decreases, further inducing the formation of a high proportion of β phase and corresponding low content of α phase. Therefore, the presence of Mo element stabilizes the β-Ti structure and promotes spontaneous passivation of the alloy. When the Mo content increases to a certain extent, only a single β phase exists in the alloy. In addition, according to the Ti-Mo phase diagram, Mo expands the gaps in the (α+β) phase region, indicating that the volume fraction of the α phase decreases with increasing Mo content.

In addition, Mo is a slowly diffusing element and has an element redistribution effect in titanium alloys, so the growth rate of the α phase is controlled by the diffusion of Mo from the α phase to the surrounding β phase. The increase of Mo element hinders the growth of α phase, resulting in the refinement of α phase size in the microstructure with the increase of Mo content.

4.2 Mechanism for synergetic improvement of strength and toughness

Due to the aforementioned microstructure changes, the mechanical properties of Ti-*x*Mo alloy system are affected by these factors, mainly including solid-solution strengthening of Mo element, refinement of β grain, and changes in α/β phase content. According to the XRD results, no alloy samples containing Mo exhibit the formation of any compounds, suggesting that Mo exists completely in the form of solid solution within the Ti lattice. Compared with Ti, Mo atoms with smaller atomic radii dissolve into the matrix phase to form a solid solution. The lattice distortion caused by the difference in atomic radius enhances the resistance to dislocation motion and promotes the increase in alloy strength.

Compared with 5Mo alloy, 6Mo alloy has achieved a synergistic improvement in strength, toughness, and plasticity, and this significant improvement in mechanical properties can be attributed to the synergistic effects of various factors. Firstly, with the increase of Mo content, the solid solution strengthening of the alloy is further enhanced, thereby improving its strength. Secondly, with the increase of Mo content, the size of β grains and α phases in the alloy further decreases, and the effect of fine grain strengthening begins to emerge, further enhancing its strength. This can be verified by the Hall-Petch formula[39,40]. However, the effects of solid solution strengthening and β grain refinement seem insufficient to explain the enhanced plasticity of 6Mo alloy. Compared with 5Mo alloy, the content of β phase in 6Mo increases. The body-centered cubic (BCC) structure of the β phase possesses a greater number of slip systems than the hexagonal close-packed (HCP) structure of the α phase. An increased number of slip systems enhances the capacity for plastic deformation and provides a greater number of pathways for dislocation movement within the metal matrix. Alloys with multiple slip systems develop a denser dislocation network, which promotes the rapid formation of dislocation entanglements and enhances the probability of dislocation interactions. These behaviors facilitate plastic deformation, thereby ultimately improving toughness.

In addition to solid solution strengthening, variations in the content and size of the α phase also play a critical role in determining the strength of titanium alloys. The β phase, characterized by its lower hardness, is the initial region to experience yield and plastic deformation during tensile testing. Conversely, the small-sized α phase within the β phase is deemed non-peelable, which inhibits the proliferation and movement of dislocations, thereby inducing β phase hardening. Furthermore, the surrounding α phase restricts the deformation of the β phase, thereby limiting dislocation motion at the α/β interface. Geometrically necessary dislocations are the result of the strain distribution and deformation between the α and β phase regions[41-43], which are crucial for improving strength. Therefore, the presence of small-sized α phases greatly enhances the strength of the alloy. More specifically, the strength will increase with the increase of α phase concentration and the decrease of α phase size. As the Mo content continues to increase, it is found that the strength-plasticity-toughness of the alloy decreases, which is attributed to the almost complete presence of β phase in the microstructure and very few α grains. Although solid solution strengthening still works, the coarsening of grains and the almost non-existent α phase make the pinning effect of a small amount of α grains ineffective during stretching, resulting in a decrease in strength instead.

Above all, the increase in Mo content means the increase in the solid solution strengthening caused by Mo element. At the same time, the increase in its content means more β phase and less α phase. The appropriate increase in solid solution strengthening will lead to the refinement of β grains, resulting in an improvement in fine grain strengthening. At the same time, the decrease in the precipitation content of α phase leads to a reduction in precipitation strengthening. Therefore, in order to achieve the best matching of strength and toughness, it is necessary to control the Mo content within a certain range, so that it has fine β grains and a certain amount of α phase, ensuring that solid solution strengthening, fine grain strengthening, and precipitation strengthening reach the equilibrium point as much as possible, thereby maximizing the strengthening effect of the alloy. For this system, the results have also summarized that when the $Mo_{[eq]}$ is 12–14, that is, the Mo content is within the range of 6wt.%–8wt.%, it can maximize the strength and toughness of titanium alloys simultaneously.

5 Conclusions

This study adopted the $Mo_{[eq]}$ method to design Ti-*x*Mo-4Al-4Zr-3Nb-2Cr-1Fe alloys, and the effect of Mo element on the phase constitution, microstructure evolution, β grain size, and corresponding strengthening and toughening mechanism of titanium alloy was explored. The main conclusions are as follows:

(1) The $Mo_{[eq]}$ value of this alloy system is between 11 and 16, and it increases linearly with the increase of Mo content. The alloys with different Mo contents exhibit a single peak of the β phase and no characteristic peaks of other phases are observed.

(2) The β grains in 5Mo alloy exhibit elongated columnar grain characteristics, with the largest grain size at about 650 μm. As the Mo content increases, the β grains transition into a more equiaxed shape in 6Mo alloy resulting in a decrease in aspect ratio and a reduction in grain size, reaching a minimum of about 362 μm at 6Mo alloy.

(3) As the Mo content increases, the α phase content gradually decreases and the α phase is almost unobservable in 9Mo alloy. The α phase in 5Mo alloy exhibits short rod-shaped shapes with an average length of about 2.4 μm, while the α phase in 6Mo alloy shows both equiaxed and short rod shape.

(4) The strength, plasticity, and toughness are the lowest in the 5Mo alloy, with values of 867 MPa, 7.3%, and 56 $MPa \cdot m^{1/2}$, respectively. However, they reach maximum in the 6Mo alloy, where the strength, plasticity, and toughness increase to 984 MPa, 12.8%, and 74 $MPa \cdot m^{1/2}$, respectively. At this point, the overall performance is the best, corresponding to a $Mo_{[eq]}$ of 12.24.

(5) The negative mixing enthalpy between Mo and other elements leads to the release of heat during the solidification process, partially offsetting the effect of structural undercooling and promoting the formation of equiaxed grains. The mechanical properties of Ti-*x*Mo alloy system are affected mainly by solid-solution strengthening of Mo element, refinement of β grain, and changes in α/β phase content.

Acknowledgments

The authors are grateful to the financial support by the National Natural Science Foundation of China (Nos. U21A2042, 52425401, U2441255, 52474377), the Major Science and Technology Achievement Transformation Project in Heilongjiang Province (No. ZC2023SH0075), and the Henan Provincial Key Research and Development & Promotion Special Program (No. 251111231400).

Conflict of interest

Prof. Rui-run Chen is an EBM of *CHINA FOUNDRY*. He was not involved in the peer-review or handling of the manuscript. The authors have no other competing interests to disclose.

References

[1] Wagih A, Mahmoud H A, Lubineau G. 3D printed auxetic metal stiffener for lightweight metal-composite T-joints with high strength and toughness. Materials & Design, 2024, 241: 112963.

[2] Huang H, Pan Y, Wang H, et al. Tough yet lightweight and flexible thermal insulative composite delivered by tendon-inspired gradient unit construction. Composites, Part B: Engineering, 2025, 292: 112088.

[3] Yang J, Lee H W, Park T M, et al. Comparative study of tensile properties and impact toughness of duplex lightweight steel. Materials Science and Engineering: A, 2024, 914: 147107.

[4] Liu L, He J, Li L, et al. Making ultrahigh-strength dual-phase steels tough: Experiment and simulation. Journal of Materials Science & Technology, 2024, 226: 302–316.

[5] Wang X Q, Han W Z. Oxygen-gradient titanium with high strength, strain hardening and toughness. Acta Materialia, 2023, 246: 118674.

[6] Li K, Zhao D, Xing Y, et al. Kink-mediated high strength and large ductility via nanocrystallization in a tough titanium alloy. Acta Materialia, 2024, 273: 119963.

[7] Zhang C, Zhang J, Bao X, et al. Hierarchically ordered coherent interfaces-driven ultrahigh specific-strength and toughness in a nano-martensite titanium alloy. Acta Materialia, 2024, 263: 119540.

[8] Qin D, Zheng L, Chen C, et al. Fracture toughness of high-strength bimodal Ti-5553 titanium alloy with pancake-shape prior β grain. Materials Science and Engineering: A, 2024, 910: 146912.

[9] Duan Q Q, Qu R T, Zhang P, et al. Intrinsic impact toughness of relatively high strength alloys. Acta Materialia, 2018, 142: 226–235.

[10] Wang Z, Bian H, Lu H, et al. Significant improvement in the strength-toughness and isotropy of laser powder bed fused Ti6Al4V alloy by combining heat treatment with subsequent laser shock peening. Materials Science and Engineering: A, 2023, 880: 145365.

[11] Wang Q, Sang B, Ren J Q, et al. Coupling effect of loading mode and temperature on the deformation behaviors of TWIP β Ti alloy: From superior tensile strength-ductility synergy to low Charpy impact toughness. International Journal of Plasticity, 2024, 174: 103920.

[12] Zhao Q, Sun Q, Xin S, et al. High-strength titanium alloys for aerospace engineering applications: A review on melting-forging process. Materials Science and Engineering: A, 2022, 845: 143260.

[13] Huang J, Bahador A, Kondoh K. Microstructure development and strengthening behaviour in hot-extruded Ti-Mo alloys with exceptional strength-ductility balance. Journal of Alloys and Compounds, 2025, 1010: 177195.

[14] Zhang C, Li X, Li S, et al. Oxygen-dislocation interaction-mediated nanotwinned nanomartensites in ultra-strong and ductile titanium alloys. Materials Today, 2024, 75: 85–96.

[15] Xu J, Zeng W, Zhu Z, et al. Morphology evolution and orientation characteristics of precipitate of ultra-high strength titanium alloy. Materials Today Communications, 2023, 36: 106619.

[16] Xie M, Huang S, Wang Z, et al. High-temperature fracture behavior of an α/β Titanium alloy manufactured using laser powder bed fusion. Acta Materialia, 2024, 277: 120211.

[17] Wang L, Fan X, Yu J, et al. Insight into the multi-hierarchical interactions between α and β phases during hot deformation of near-β titanium alloy. Materials Science and Engineering: A, 2024, 903: 146649.

[18] Zhu K, Huang J, Nie W, et al. Ultrahigh yield strength heterostructured titanium matrix composites by controlling the α/α′ precipitation sequence. Journal of Alloys and Compounds, 2024, 1004: 175886.

[19] Antonov S, Shi R, Li D, et al. Nucleation and growth of α phase in a metastable β-Titanium Ti-5Al-5Mo-5V-3Cr alloy: Influence from the nano-scale, ordered-orthorhombic O″ phase and α compositional evolution. Scripta Materialia, 2021, 194: 113672.

[20] Pang H, Luo J, Li C, et al. The role of β phase in the morphology evolution of α lamellae in a dual-phase titanium alloy during high temperature compression. Journal of Alloys and Compounds, 2022, 910: 164901.

[21] Zhu C, Zhang X Y, Li C, et al. A strengthening strategy for metastable β titanium alloys: Synergy effect of primary α phase and β phase stability. Materials Science and Engineering: A, 2022, 852: 143736.
[22] Yao Z, He M, Yi J, et al. High-strength titanium alloy with hierarchical-microstructure design via in-situ refinement-splitting strategy in additive manufacturing. Additive Manufacturing, 2024, 80: 103969.
[23] Tan C, Yang T, Huang C, et al. Enhanced strength-ductility synergy in Ti55531 titanium alloys through gradient microstructural design strategy. Materials Science and Engineering: A, 2024, 909: 146823.
[24] Sun S, Xu Z, Wu B, et al. A new design method for Ti-VMoCrFeAl titanium alloys with superb strength. Materials Science and Engineering: A, 2025, 922: 147627.
[25] Zhang J, Guo H, Hu M, et al. Effect of common alloying elements on α' martensite start temperature in titanium alloys. Journal of Materials Research and Technology, 2023, 27: 4562–4572.
[26] Huang S, Zhao Q, Yang Z, et al. Strengthening effects of Al element on strength and impact toughness in titanium alloy. Journal of Materials Research and Technology, 2023, 26: 504–516.
[27] Pang X, Yao C, Xiong Z, et al. Comparative study of coatings with different molybdenum equivalent on titanium alloy forged plate for laser cladding: Microstructure and mechanical properties. Surface and Coatings Technology, 2022, 446: 128760.
[28] Li H, Cai Q, Li S, et al. Effects of Mo equivalent on the phase constituent, microstructure and compressive mechanical properties of Ti-Nb-Mo-Ta alloys prepared by powder metallurgy. Journal of Materials Research and Technology, 2022, 16: 588–598.
[29] Yang Y L, Wang W Q, Li F L, et al. The effect of aluminum equivalent and molybdenum equivalent on the mechanical properties of high strength and high toughness titanium alloys. Materials Science Forum, 2009, 618–619: 169–172.
[30] Manda P, Pathak A, Mukhopadhyay A, et al. Ti-5Al-5Mo-5V-3Cr and similar Mo equivalent alloys: First principles calculations and experimental investigations. Journal of Applied Research and Technology, 2017, 15(1): 21–26.
[31] Guo Y, Niu J, Cao J, et al. Relative strength of β phase stabilization by transition metals in titanium alloys: The Mo equivalent from a first principles study. Materials Today Communications, 2023, 35: 106123.
[32] Li Y L, Fang H Z, Zhang X F, et al. Forming mechanism of growth twins and microstructure evolution on improvement of strength and toughness properties by β-eutectoid element in Ti-7Mo-4Al-4Zr-3Nb-2Cr-*x*Fe alloys. Journal of Alloys and Compounds, 2023, 947: 169507.
[33] Akmal M, Hussain A, Afzal M, et al. Systematic study of $(MoTa)_xNbTiZr$ medium- and high-entropy alloys for biomedical implants-In vivo biocompatibility examination. Journal of Materials Science & Technology, 2021, 78: 183–191.
[34] Wang T, Guo H, Tan L, et al. Beta grain growth behaviour of TG6 and Ti17 titanium alloys. Materials Science and Engineering: A, 2011, 528(21): 6375–6380.
[35] Gil F X, Rodríguez D, Planell J A. Grain growth kinetics of pure titanium. Scripta Metallurgica et Materialia, 1995, 33(8): 1361–1366.
[36] Gil F J, Planell J A. Behaviour of normal grain growth kinetics in single phase titanium and titanium alloys. Materials Science and Engineering: A, 2000, 283(1–2): 17–24.
[37] Rietveld H M. A profile refinement method for nuclear and magnetic structures. Journal of Applied Crystallography, 1969, 2(2): 65–71.
[38] Zhao Y Q, Xin S W, Zeng W D. Effect of major alloying elements on microstructure and mechanical properties of a highly β stabilized titanium alloy. Journal of Alloys and Compounds, 2009, 481(1–2): 190–194.
[39] Li S, Li S, Liu L, et al. High-temperature "Inverse" Hall-Petch relationship and fracture behavior of TA15 alloy. International Journal of Plasticity, 2024, 176: 103951.
[40] Wu Z, Turner R, Qi M, et al. Effect of phase boundary on the critical resolved shear stress and dislocation behavior of dual-phase titanium alloy. Acta Materialia, 2024, 275: 120051.
[41] Han Q, Lei X, Yang H, et al. Effects of temperature and load on fretting fatigue induced geometrically necessary dislocation distribution in titanium alloy. Materials Science and Engineering: A, 2021, 800: 140308.
[42] Zhong H, Shi Q, Dan C, et al. Resolving localized geometrically necessary dislocation densities in Al-Mg polycrystal via in situ EBSD. Acta Materialia, 2024, 279: 120290.
[43] Zhu C, Livescu V, Harrington T, et al. Investigation of the shear response and geometrically necessary dislocation densities in shear localization in high-purity titanium. International Journal of Plasticity, 2017, 92: 148–163.